Stall Delay of Two-Wing Configurations with Decalage at Low Reynolds Numbers

R. Jones[1], D. J. Cleaver[2] and I. Gursul[3]
Department of Mechanical Engineering, University of Bath, Bath, BA2 7AY, UK

Nomenclature

b = semi-span

c = chord

C_D = time-averaged drag coefficient, $D/q_\infty cb$

C_L = time-averaged lift coefficient, $L/q_\infty cb$

q_∞ = freestream dynamic pressure, $\rho U_\infty^2/2$

Re = Reynolds number, $\rho U_\infty c/\mu$

U = streamwise component of flow velocity

U_∞ = freestream velocity

V = crosswise component of flow velocity

X = longitudinal/streamwise coordinate

Y = transverse/crosswise coordinate

α = angle of attack

$\Delta X/c$ = dimensionless stagger

$\Delta Y/c$ = dimensionless gap

μ = dynamic viscosity

ρ = freestream density

Subscripts

m = monoplane

t = two wing

1 = leading wing

2 = trailing wing

---

[1] Postgraduate Student, Department of Mechanical Engineering. Student Member AIAA.
[2] Lecturer, Department of Mechanical Engineering. Member AIAA.
[3] Professor, Department of Mechanical Engineering. Associate Fellow AIAA.

I. Introduction

NUMEROUS potential operations have been proposed for Micro Air Vehicles (MAVs) both military and civil. With the current climate of global conflicts MAVs will likely have an instrumental future in the modern world [1, 2]. However, MAVs continue to face significant performance challenges. The tendency for flow separation over the lifting surfaces poses as the most significant challenge due to the low Reynolds number aerodynamics [3].The stall angle of attack of single wings is lower, making them prone to gust-induced stall [4]. With the stringent size and weight constraints (15 cm span and 100g) and the poor lifting performance of wings at low Reynolds numbers, current designs of MAVs fall significantly short of the required performance [5]. It has been postulated that MAVs would frequently need to fly at high angles of attack, close to stall conditions, in order to compensate for their poor lifting performance [6]. In addition, low flight speeds may be preferable for visual surveillance and controllability. Post-stall flight would therefore be inevitable during high angle of attack maneuvers and vertical gusts. Hence, the delay of stall in MAV design is crucial.

Two-wing configurations could offer a low cost and efficient means of increasing the lifting area. Historically, biplane wings offered increased planform area and increased structural rigidity through inter-wing bracing. With the development of monoplane aircraft, biplane aircraft were largely relegated to sport aviation [7, 8]. However, previous studies have demonstrated that two wing configurations can delay stall at low Reynolds numbers [1, 9]. Staggered biplanes ($\Delta X/c$ = 0.5) were noted to show the most significant stall delay for a wing gap of $\Delta Y/c$ = 0.85. Stall was delayed by 10° resulting in a $C_{L,max}$ = 0.97 compared to $C_{L,max}$ = 0.79 for the single wing (see Fig. 1; from ref. [1]). The corresponding benefits in aerodynamic and power efficiency were 5 and 20% respectively. This stall delay was due to strong inter-wing flow aft of the upper/leading wing which strongly suppressed the separated flow over the lower/trailing wing. In this case, both wings had the same angle of attack.

Several studies have considered the effects of decalage (differing wing angle: $\delta = \alpha_1 - \alpha_2$) [7, 10, 11]. However, many of these studies only consider the effects at large gaps or stagger (typically fixed at or above one chord) missing the region of greatest potential improvement [1]. In addition, there is little information on the flow fields and with the limited number of variations in decalage it is difficult to gauge the significance of decalage from previous studies [7, 10, 11].

This study investigates the effects of decalage in two-wing configurations with relatively small gaps and stagger. The aim is to enhance the stall delay of MAV flight. The optimised stall delay to 25° has been observed for stagger

$\Delta X/c$ = 0.5 and gap $\Delta Y/c$ = 0.85 [1]. Hence, this configuration (with zero-decalage) is treated as the baseline configuration. The suppression of the separated flow over the lower/trailing wing was noted to be a significant factor in the stall delay of two-wing configurations (see Fig. 1) [1]. For this reason, the trailing wing's incidence was fixed at 25° and the leading wing with variable incidence was positioned so that its wake interacted with the separated shear layer of the fixed-trailing wing (see Fig. 2a). The following sections present force and flow field measurements which reveal new insight into the effects of decalage in two-wing configurations.

II. Experimental Techniques

Force and particle image velocimetry (PIV) measurements were performed in a low-speed, low turbulence return-circuit open-jet wind tunnel at the University of Bath, Mechanical Engineering Department. The turbulence intensity is 0.1% at a maximum freestream speed of 30 ms^{-1}. The freestream velocity was U_∞ = 15 ms^{-1} with a chord Reynolds number of Re = 10^5. Figure 2a shows the two-wing geometries considered. The wing stagger was $\Delta X/c$ = 0.5, the leading wing incidence was varied from $\alpha_1 = -10°$ to 30° in 5° intervals, the trailing wing was fixed at α_2 = 25° and the gap ranged between $\Delta Y/c$ = 0 and 1.5. Figure 2b shows the test rig in situ with PIV equipment also illustrated. Cantilever flat-plate wing models with semi-span b = 200 mm and chord c = 100 mm (sAR = 2) protruded through an endwall symmetry plane. The wings had square edges, a thickness of 2.5% chord and were inflexible in both chordwise and spanwise directions.

The lift and drag forces were measured using a pair of two component aluminum binocular force balances which provided the lift and drag data on the wings individually. The forces were measured by amplification of the strain gauge signals in full Wheatstone bridge circuits. The measurement range of the load cells was ± 8 N in the lift component and ± 6 N in the drag component. Force versus voltage calibration data was collected before and after each data acquisition to ensure validity and accuracy. The uncertainty in lift and drag coefficient was ± 2 %. The wing models were traversed in the crosswise direction with off-the-shelf linear actuators from HepcoMotion®. A pair of linear displacement transducers configured in full Wheatstone bridge circuits provided the relative position of the wings. Displacement versus voltage calibration data were likewise collected at regular intervals and the uncertainty in the computed transverse wing separation was ± 1 %.

The Particle Image Velocimetry measurements were conducted using a 120 mJ pulsed laser at 15 Hz. The measurement plane was the mid-span plane of the wings. A 4 MP camera and TSI® LaserPulse synchronizer were

used to capture 200 images pairs, which were then analyzed using TSI's Insight3G software with a fast Fourier transform cross-correlation algorithm. The uncertainty of the PIV measurements is around ±2 % of the freestream velocity. A complete description of the measurement apparatus and uncertainties are described elsewhere [1, 12, 13].

III. Results

Section A shall discuss the total force coefficients of two-wings with decalage variations as a function of gap. Section B shall discuss the flow fields in conjunction with the lift coefficient of the separate wings. Comparisons are made to the zero-decalage configuration with maximum lift (the baseline configuration) which occurs for $\alpha = 25°$ and $\Delta Y/c = 0.85$ [1].

A. Force Measurements

Figure 3 shows the total lift coefficient ($C_{Lt} = (C_{L1} + C_{L2}) / 2$) as a function of positive gap. At small gaps ($\Delta Y/c < 0.2$), the total lift coefficient lies between $C_{Lt} = 0.3$ to 0.6 for all α_1. As the gap increases, the total lift coefficient increases reaching distinct local maxima. The zero-decalage case ($\alpha_1 = 25°$; $\delta = 0°$) produces a maximum total lift coefficient of $C_{Lt} = 0.93 \pm 0.02$ at a gap of $\Delta Y/c = 0.85$. In negative decalage cases with $5° \leq \alpha_1 \leq 20°$, the total lift coefficient exceeds the zero-decalage configuration's maximum lift coefficient. Moreover, as the incidence of the leading wing decrease below $\alpha_1 = 25°$, the lift maxima occur at smaller gaps relative to the baseline configuration. The most significant local maximum in total lift occurs for $\alpha_1 = 15°$ at $\Delta Y/c = 0.55$ ($C_{Lt} = 1.02 \pm 0.02$) which exceeds the zero-decalage lift peak by 9%.

Figure 4 shows the total lift, drag, aerodynamic efficiency and power efficiency coefficients versus α_1 for the cases of maximum lift from Fig. 3. For leading wing angles of attack around the optimal angle ($\alpha_1 = 15°$), the total lift is larger than that of the baseline configuration. Interestingly, the maximum aerodynamic and power efficiency occur when $\alpha_1 < 15°$, due to the smaller drag coefficient in this range. For example, at $\alpha_1 = 10°$ the maximum lift coefficient occurs at $\Delta Y/c = 0.45$ which yields the greatest power efficiency (46% larger than the baseline configuration). At $\alpha_1 = 5°$, the maximum lift coefficient occurs at $\Delta Y/c = 0.4$ which yields the highest aerodynamic efficiency (54% larger than the baseline configuration).

Figure 5 shows the lift coefficient of the separate wings and total lift coefficient versus α_1 for gaps of maximum lift. The peak in total lift coefficient at $\alpha_1 = 15°$ is attributable to a dominance in leading wing lift which emerges in

the $10° \leq \alpha \leq 20°$ range (see Fig. 5). For leading wing angles of attack between $-10° \leq \alpha_1 \leq 10°$, the leading wing lift is linear. Interestingly, at $\alpha_1 = 0°$ the leading wing produces a lift coefficient of $C_{L1} = 0.55 \pm 0.01$. This is comparable to the lift coefficient measured for a single wing at $\alpha = 8°$ ($C_{Lm} = 0.53 \pm 0.02$). Hence, the presence of the trailing wing augments the leading wing's lift.

B. Velocity Measurements

Flow fields for the specific angles of attack of unfixed wing α_1 and gaps shown in Figure 5 were investigated. Figure 6 shows the corresponding flow fields for gaps of maximum lift. For configurations which have negative or zero leading wing incidence ($\alpha_1 = -10°, -5°, 0°$), the maximum lift evidently occurs when the wings are almost touching (Fig. 6, top row), thus limiting the amount of inter-wing flow.

As noted previously, the configurations with $\alpha_1 = 5°$, 10° and 15° produce better aerodynamic efficiency, power efficiency and total lift coefficient. Analysis of the flow fields (see Fig. 6, middle row) reveals that these configurations exhibit strong downwash and deflection of the leading wing's separated shear layer via the interaction with the accelerated inter-wing flow. Hence, the separated recirculation regions of both wings are suppressed. This wake suppression is most significant over the trailing wing which is in sharp contrast with the single wing at the same angle (Fig. 1b).

The lift coefficient of the upper/leading wing drops rapidly below the lower/trailing wing's lift coefficient for $\alpha_1 > 15°$ (Fig. 5). This correlates with deflection of the leading wing's trailing-edge shear layer. This becomes noticeable once α_1 reaches 15° (see Figure 6) and intensifies at higher angles of attack ($\alpha_1 = 20°$, 25° and 30°) as shown in bottom row of Fig. 6. However, the deflection of the leading-edge shear layer of the leading wing is less apparent compared to the configuration at $\alpha_1 = 15°$. Hence, the recirculation regions are larger. These are likely key factors in reducing the leading wing's lift coefficient.

The influence of the interaction on the trailing wing is also noteworthy. In contrast to the lift of the leading wing, as the incidence increases above $\alpha_1 = 15°$ (Fig. 6, middle and bottom rows), the lift coefficient of the trailing wing continues to increase. Analysis of the flow over the trailing wings' suction surfaces reveals that the wake and recirculation regions are comparable in size to that of the leading wing at $\alpha_1 = 10°$. Evidently, as the leading wing's

incidence increases, the maximum lift coefficients are observed to occur at increasing values of gap. The inter-wing flow increases in speed as the leading wing incidence increases. As a result, the lift of the trailing wing also increases.

IV. Conclusions

Force measurements revealed significantly enhanced performance in lift coefficient, aerodynamic efficiency and power efficiency in configurations with distinct local maxima in lift coefficient at *optimal* gaps. For decalage configurations with $\alpha_1 \leq 20°$, these local maxima occurred at smaller gaps compared to the zero-decalage case. In some cases ($10° \leq \alpha_1 \leq 20°$), the lift maxima exceeded that of the baseline configuration reaching a 9% increase in total lift coefficient at $\alpha_1 = 15°$ and $\Delta Y/c = 0.55$. Gaps of maximum aerodynamic and power efficiency exceeded the zero-decalage baseline configuration by 54% and 46% respectively. These benefits were found at smaller gaps relative to the baseline configuration. Hence, the use of decalage can not only augment the performance of micro air vehicles (MAVs), but also reduce the required volume occupied by the lifting surfaces.

Particle image velocimetry measurements revealed that configurations producing enhanced lift, aerodynamic and power efficiency were associated with deflected shear layers and smaller wakes due to the accelerated inter-wing flow. Hence, the interaction of separated flow of the leading wing with the trailing wing is important. The results presented in this paper demonstrate that MAV performance can be significantly enhanced with the use of decalage. This could not only augment general performance in terms of climb rate and turning circle, but also control stall during gusts. An adaptive configuration with variable angle of attack of the leading wing could be considered for future applications.

Acknowledgments

This work was funded by the University of Bath University Research Scholarship award. The authors would like to acknowledge the University of Bath's technical support staff for their continued support.

References

1. Jones, R., Cleaver, D. J., and Gursul, I. "Aerodynamics of biplane and tandem wings at low Reynolds numbers," *Experiments in Fluids*, Vol. 56, No. 6, 2015, pp. 1-25. doi: 10.1007/s00348-015-1998-3

2. Mueller, T. J., and DeLaurier, J. D. "Aerodynamics of small vehicles," *Annual Review of Fluid Mechanics*, Vol. 35, No. 1, 2003, pp. 89-111. doi: 10.1146/annurev.fluid.35.101101.161102

3. Kunz, P. J., and Kroo, I. "Analysis and design of airfoils for use at ultra-low Reynolds numbers," *Fixed and Flapping Wing Aerodynamics for Micro Air Vechicle Applications*. Vol. 195, Progress in Astonautics and Aeronautics, AIAA, Reston, VA, USA, 2001, pp. 35-59.

4. Gursul, I. "Vortex flows on UAVs: Issues and challenges," *Aeronautical Journal*, Vol. 108, No. 1090, 2004, pp. 597-610.

5. Pines, D. J., and Bohorquez, F. "Challenges facing future micro-air-vehicle development," *Journal of aircraft*, Vol. 43, No. 2, 2006, pp. 290-305. doi: 10.2514/1.4922

6. Cleaver, D. J., Wang, Z., Gursul, I., and Visbal, M. R. "Lift enhancement by means of small-amplitude airfoil oscillations at low Reynolds numbers," *AIAA Journal*, Vol. 49, No. 9, 2011, pp. 2018-2033. doi: 10.2514/1.J051014

7. Khan, F. A., and Mueller, T. J. "Tip vortex/airfoil interaction for a low Reynolds number canard/wing configuration," *Journal of Aircraft*, Vol. 28, No. 3, 1991, pp. 181-186. doi: 10.2514/3.46010

8. Traub, L. W. "Theoretical and experimental investigation of biplane delta wings," *Journal of Aircraft*, Vol. 38, No. 3, 2001, pp. 536-546. doi: 10.2514/2.2794

9. Kang, H., Genco, N., and Altman, A. "Gap and stagger effects on biplanes with end plates part I," 47th AIAA Aerospace Sciences Meeting and Exhibit, Orlando, FL, USA, AIAA Paper 2009-1085, 2009.

10. Knight, M., and Noyes, R. W. "Wind tunnel pressure distribution tests on a series of biplane wing models Part II: effects of changes in decalage, dihedral, sweepback and overhang." NACA-TN-325, 1929.

11. Scharpf, D. F., and Mueller, T. J. "Experimental study of a low Reynolds number tandem airfoil configuration," *Journal of Aircraft*, Vol. 29, No. 2, 1992, pp. 231-236. doi: 10.2514/3.46149

12. Jones, R., Cleaver, D. J., and Gursul, I. "Fluid-structure interactions for flexible and rigid tandem-wings at low Reynolds numbers," 53rd AIAA Aerospace Sciences Meeting, Kissimmee, FL, USA, AIAA Paper 2015-1752, 2015.

13. Jones, R. "Aerodynamics of biplane and tandem wings at low Reynolds numbers," Ph.D. Thesis, Dept of Mechanical Engineering, Univ. of Bath, Bath, England, U.K., 2016.

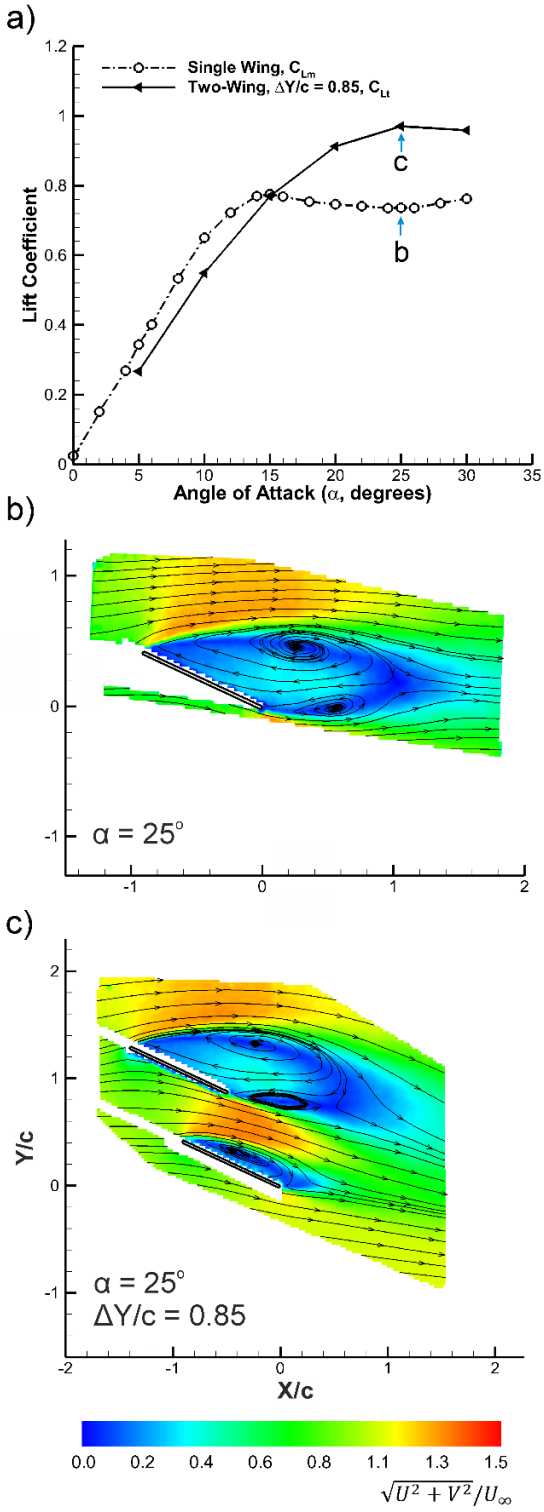

Fig. 1 a) Stall delay for optimal two wing configurations without decalage compared to a single wing. b) Flow field for a single wing in deep stall. c) Flow field for two wings at maximum lift demonstrating stall delay. From Jones et al. [1].

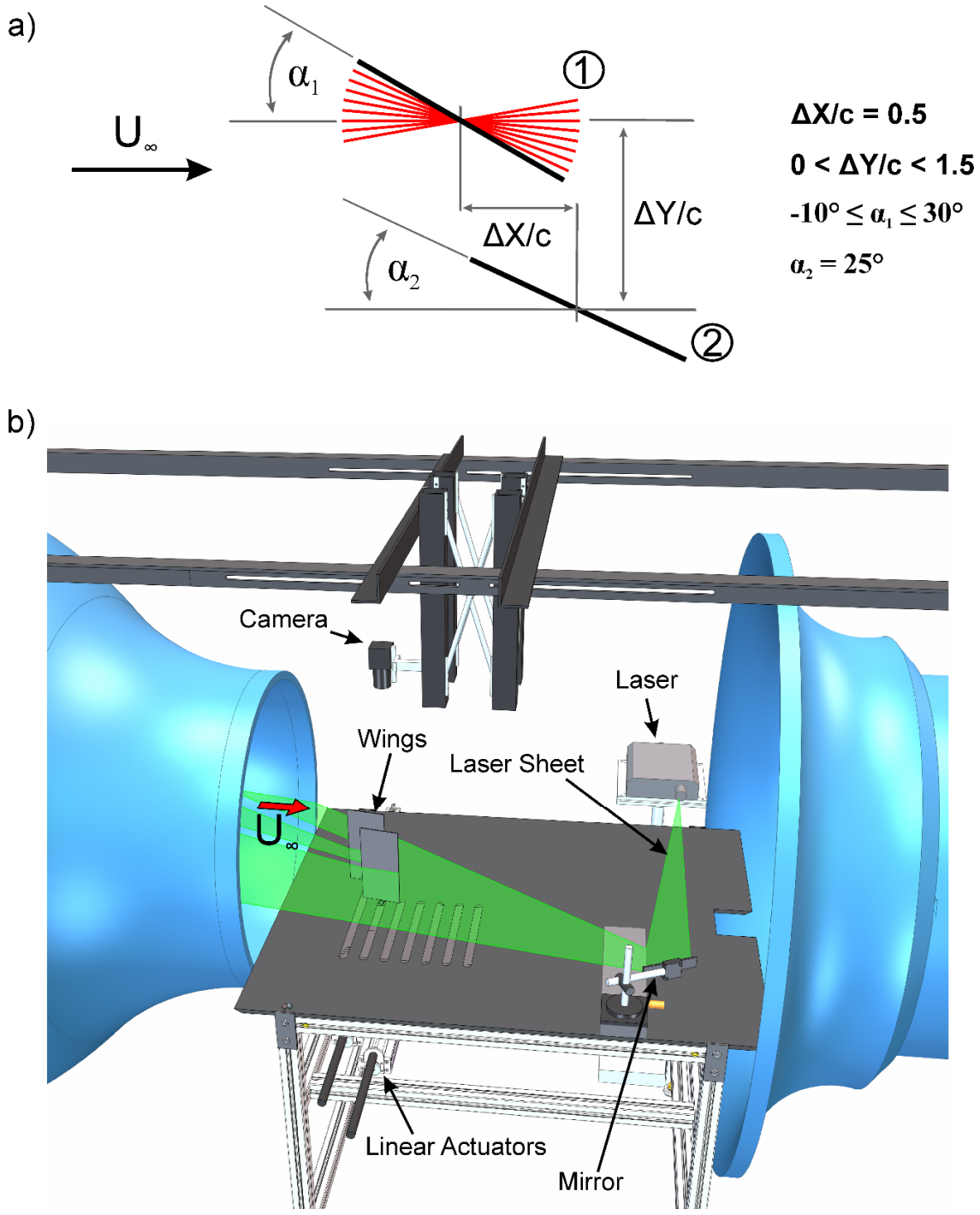

Fig. 2 a) Geometric illustration of the decalage configurations considered in this article. b) Experimental setup in-situ.

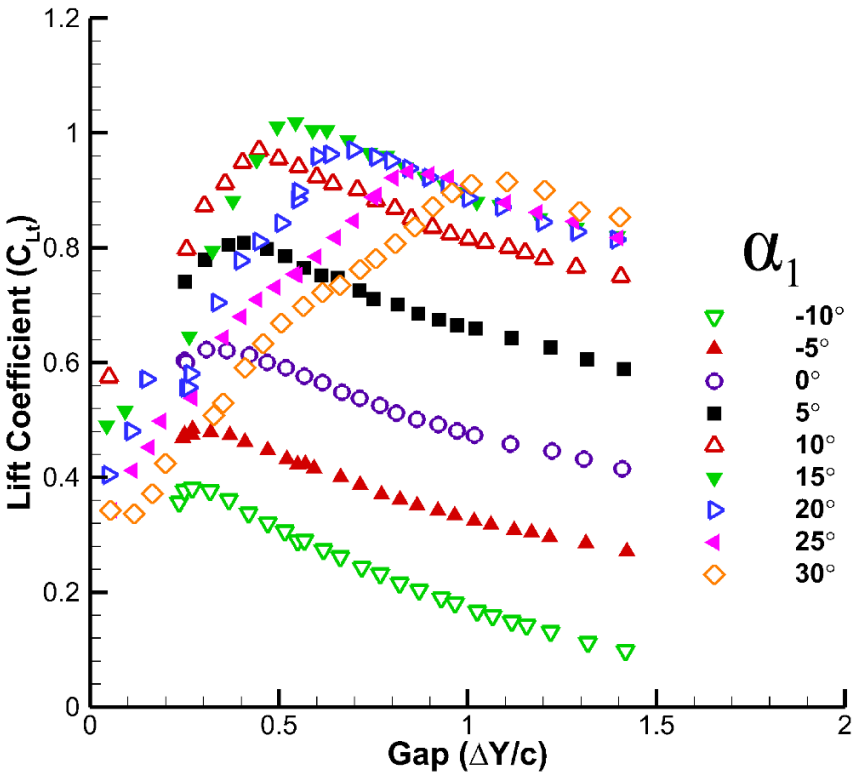

Fig. 3 Total lift coefficient versus gap for two-wing decalage configurations. The leading wing incidence (α_1) is varied while the trailing wing incidence (α_2) is fixed at 25°. $\Delta X/c$ = 0.5.

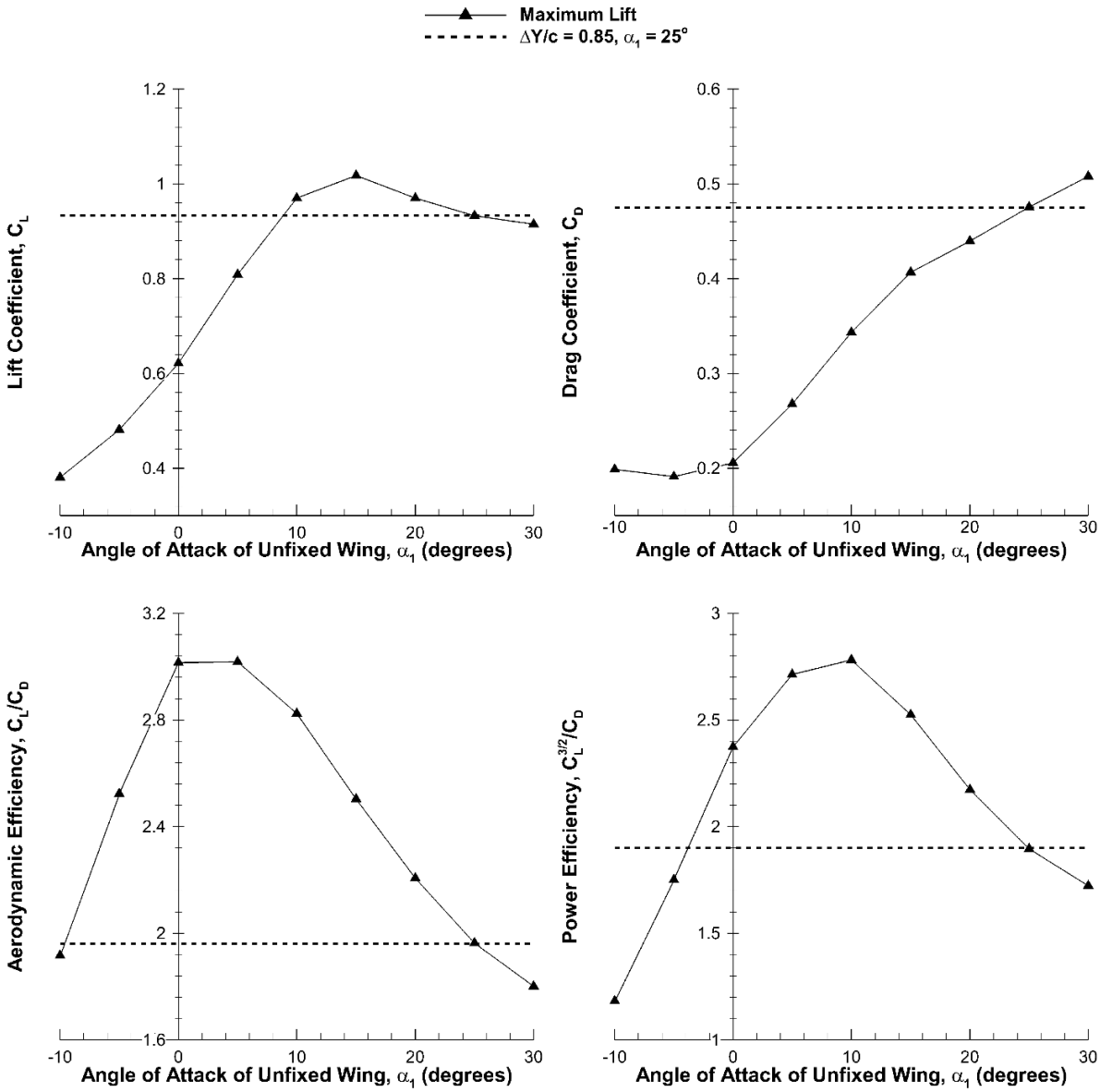

Fig. 4 Total lift and drag coefficient, aerodynamic and power efficiency versus angle of attack of the variable incidence wing for configurations producing maximum lift. The dashed line represents the baseline configuration.

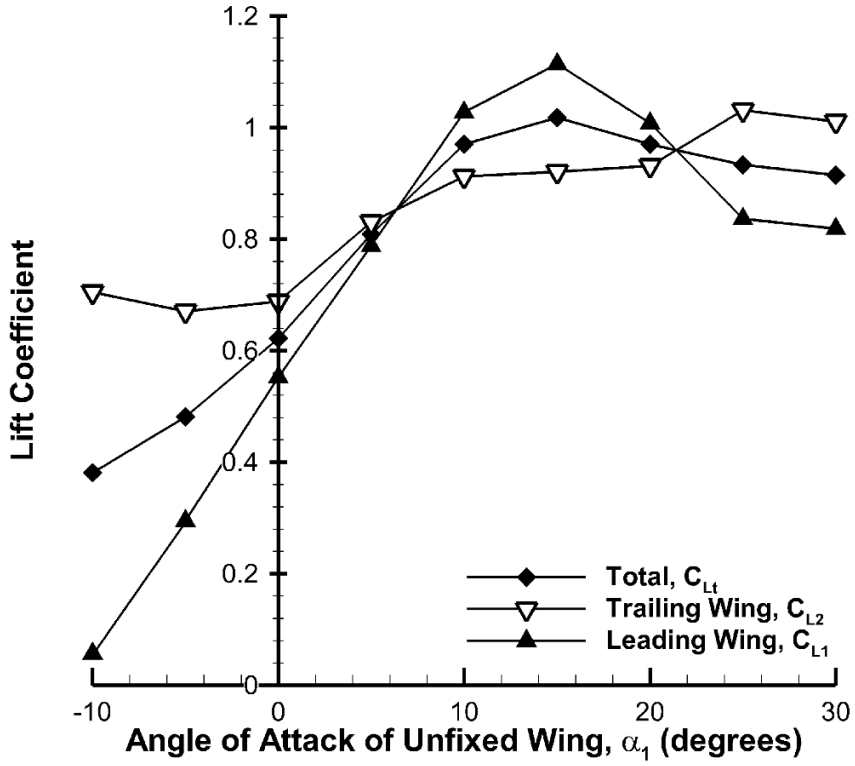

Fig. 5 Lift coefficients of the leading wing, trailing wing and total versus angle of attack of the variable incidence wing for gaps with maximum lift.

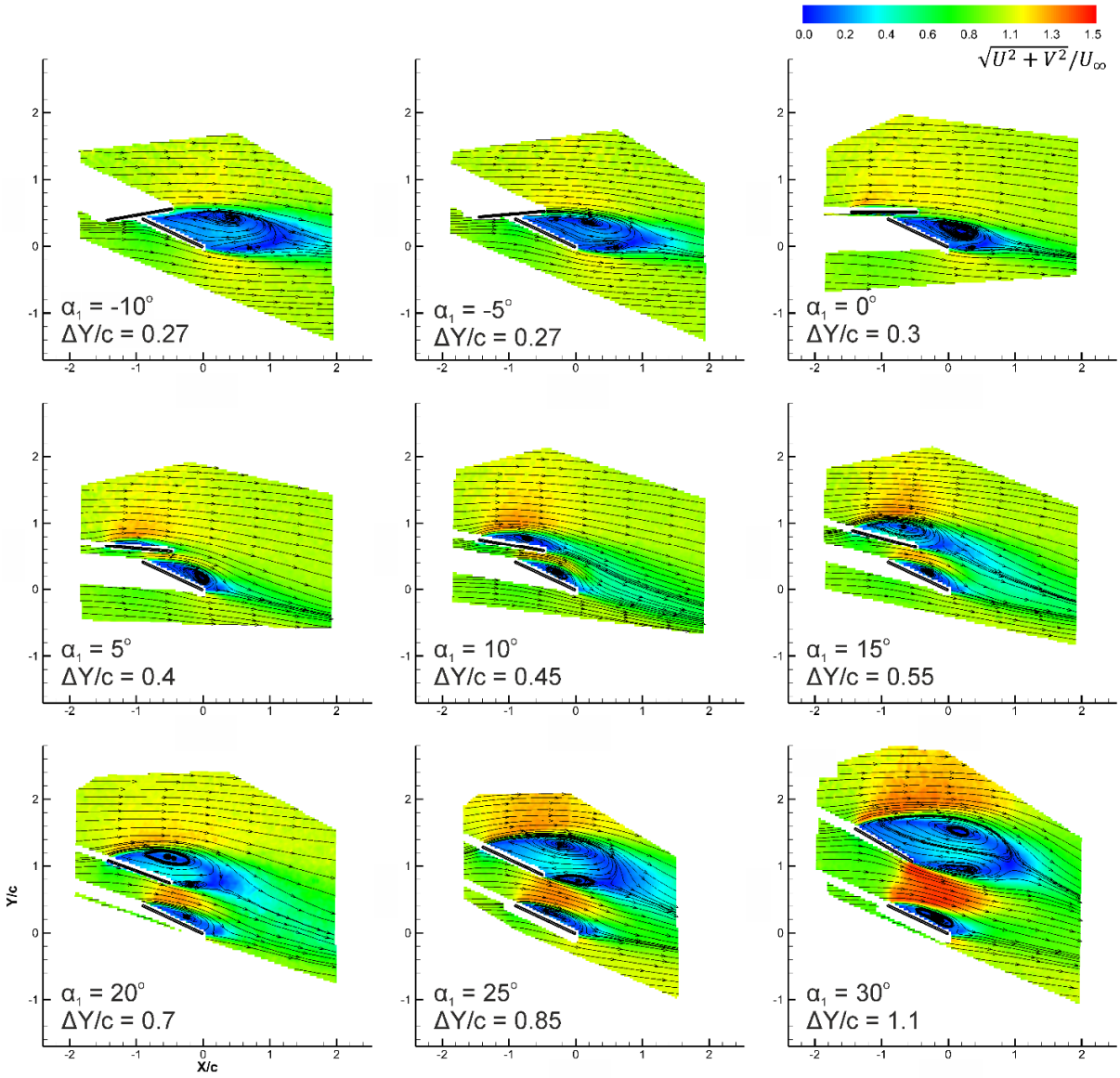

Fig. 6 Time averaged velocity magnitude as a function of incidence of the leading wing. Configurations correspond to the optimal gaps that produce maximum lift for each incidence as shown in Figs. 4 and 5.